Supporting Information

Moglie et al. 10.1073/pnas.1719077115

SI Methods

Electrophysiological Recordings from IHCs and Afferent Postsynaptic Boutons. Euthanasia and tissue extraction were carried out according to approved animal protocols (INGEBI and Johns Hopkins Institutional Animal Care and Use Committees). Excised apical turns of 9- to 11-d-old mouse cochleae (BALB/c or FvB mice, either sex) were placed into a chamber on the stage of an upright microscope (Olympus BX51WI) and used within 2 h. Mice were used in all cases, except for afferent bouton recordings and EM, where Sprague–Dawley rat cochleae were used (Figs. 3, 5, and 6 and Fig. S6). IHCs and contacting postsynaptic terminals were visualized on a monitor via a water immersion objective (60× magnification), differential interference contrast optics, and a CCD camera (Andor iXon 885). Supporting tissue was removed to access IHCs and afferent boutons. All recordings were performed at room temperature (22–25 °C).

The cochlear preparation was superfused continuously at 2–3 $mL{\cdot}min^{-1}$ with extracellular saline solution of an ionic composition similar to that of the perilymph: 144 mM NaCl, 5.8 mM KCl, 1.3 mM $CaCl_2$, 0.7 mM NaH_2PO_4, 5.6 mM D-glucose, and 10 mM Hepes buffer (pH 7.4). Ca^{2+} buffering and current-clamp experiments (Figs. 7 and 8 and Fig. S4) were performed with the addition of 0.9 mM $MgCl_2$. Working solutions containing different drugs were made up in this same saline and delivered through the perfusion system.

Recording pipettes were fabricated from 1-mm borosilicate glass (WPI), with tip resistances of 9–12 (bouton) and 6–8 (IHC) MΩ. Pipettes used for bouton recordings were Sylgard-coated and fire-polished. Series resistance errors were not compensated for.

For afferent bouton and current-clamp recordings (Figs. 5–7 and Figs. S4 and S6), the pipette solution contained the following: 140 mM KCl, 5 mM Hepes buffer, 2.5 mM Na_2ATP, 5 mM phosphocreatine-Na_2, 5 mM EGTA, 3.5 mM $MgCl_2$, and 2 mM$CaCl_2$ (pH 7.2). Ca^{2+} imaging (Figs. 1, 2, and 4 and Figs. S2, S5, and S7) and Ca^{2+} buffering (Fig. 8) experiments were performed with an intracellular solution made from 2× stock to reach a final concentration of 140 mM KCl, 5 mM Hepes buffer, 2.5 mM Na_2ATP, 5 mM phosphocreatine-Na_2, and 3.5 mM $MgCl_2$ (pH 7.2). EGTA, BAPTA, and/or 0.4 mM Ca^{2+} indicator (Fluo-4 or Fluo-5F; Invitrogen) was added at the indicated concentrations. In the experiments shown in Fig. 2 and Fig. S1, a RIBEYE peptide conjugated to rhodamine, developed by Zenisek et al. (68) and acquired at Genscript, was included in the intracellular solution to a final concentration of 40 μM. In Ca^{2+} buffering experiments, $CaCl_2$ was also added to reach an estimated 100 nM free Ca^{2+} concentration. For perforated-patch recordings, pipette tips were first dipped for 2 min in an intracellular solution devoid of amphotericin and then backfilled with the intracellular solution containing 400 μg/mL amphotericin B (Calbiochem). Unless otherwise stated, all drugs were acquired from Sigma.

Efferent synaptic currents were evoked by unipolar electrical stimulation of the MOC efferent axons as described previously (32). Briefly, the electrical stimulus was delivered via a 20- to 80-μm-diameter glass pipette placed at 20–60 μm modiolar to the base of the IHC under study. The position of the pipette was adjusted until postsynaptic currents in the IHC were consistently activated. An electrically isolated constant current source (model DS3; Digitimer) was triggered via the data acquisition computer to generate pulses of 40–180 μA, with a 2-ms width. Solutions containing ACh or K^+ (25 mM) were applied by a gravity-fed multichannel glass pipette (150-μm tip diameter). Electrophysiological recordings in IHCs and afferent boutons were performed using a Multiclamp 700B amplifier (Molecular Devices), low-pass-filtered at 2–10 kHz, and digitized at 50 kHz via a National Instruments board. Data were acquired using WinWCP (J. Dempster, University of Strathclyde, Glasglow, Scotland). IHC recordings were analyzed with custom-written routines in IgorPro 6.37 (Wavemetrics), and EPSCs were analyzed with bouton recordings using Mini Analysis (Synaptosoft). Statistical analysis was performed using Infostat (Universidad Nacional de Córdoba). Errors are SEM unless otherwise stated.

Ca^{2+} Imaging Experiments. Ca^{2+} indicators were included in the patch pipettes, allowing diffusion into the cells. The preparation was illuminated with a blue LED system (Tolket), and images were acquired using an Andor iXon 885 camera controlled through a Till Photonics interface system. The focal plane was located close to the basal pole of the IHC. The signal-to-noise ratio was improved with a chip binning of 4 × 4, giving a resolution of 0.533 μm per pixel using a 60× water immersion objective. The image size was set to 100 × 100 pixels, which allowed an acquisition rate of 140 frames per second. Image acquisition started 5 min after whole-cell break-in to ensure proper dialysis of the cell content and lasted up to 40 min.

Images were analyzed with custom-written routines in IgorPro 6.37. An initial image of the IHC basal pole, obtained by epifluorescence (Fig. S1*A*), was used to create a donut-shaped mask covering the cell's cytoplasm around the nucleus, which was left out of the analysis (typically, the nucleus featured the highest fluorescence intensity). The center of the mask was set at the maximal intensity pixel of the cell, and the inner and outer circumferences of the donut corresponded to 40–90% of the maximal fluorescence intensity (Fig. S1*B*). Then, the mask was divided in 36 radial ROIs across the IHC cytoplasm (Fig. S1*C*), and the mean $\Delta F/F_0$ (%) was calculated in every ROI for each time frame. We considered that there was a significant increase in fluorescence in a particular ROI in those cases where the peak fluorescence signal detected after electrical stimulation was threefold higher than the SD of the baseline and the integral of the fluorescence signal was above 0.3 (arbitrary units × seconds). Finally, those ROIs that exhibited a consistent pattern of activation were selected as hotspots. Photobleaching was corrected for long-acquisition protocols performed in Figs. 4 and 8 *A* and *B* and Figs. S5 and S7 by fitting a line between the prestimulus baseline and final fluorescence. Unlike the rest of the study, fluorescence signals in the experiments shown in Fig. 8 were not normalized to F_0 to avoid distortions produced by the increased basal fluorescence signal during the application of the Ca^{2+}-ATPase inhibitor CPA (69).

Experiments in Fig. 2 and Fig. S2 were performed in an upright microscope (Nikon Eclipse E660FN) coupled to a swept-field confocal scanner (Prairie Technologies) and illuminated with a 200-mW argon laser at 488 nm (Agilent Technologies). Acquisition of the fluorescently labeled RIBEYE peptide signal was performed using 561-nm laser illumination. Confocal images were captured with an Andor DU-897 X-8853 camera at an acquisition rate of 110 frames per second. We used the 50-μm slit diffraction limited in the object plane, which allowed us to get a good signal-to-noise ratio with an exposure time of 8 ms. A lateral resolution of 0.27 μm per pixel was obtained with a Nikon 60× objective (N.A. = 1). Focal planes were taken in 0.5-μm steps, and images were acquired with NIS-Elements Software (Nikon). Images

were analyzed with custom-written routines in IgorPro 6.37 and ImageJ (NIH). The peak response image for each stimulation protocol in every plane was obtained and used to make a 3D reconstruction of the IHC. Measurement of the point spread function of the imaging system using 0.175-μm-diameter fluorescent beads (PS-Speck; Molecular Probes) allowed us to perform a deconvolution of the reconstructed IHC using the Parallel Iterative Deconvolution plug-in in ImageJ. Then, a Laplacian of Gaussian filter (70, 71) was applied to highlight regions of rapid intensity change. Efferent and afferent Ca^{2+} entry hotspots were detected using a threshold-based criterion (72).

EM. Serial section EM was carried out on midturn cochlear segments from two Sprague–Dawley rat pups (9 d after birth). Tissue was obtained and processed according to published methods (51). In brief, the temporal bone was excised and tissue was fixed by perfusion through the round window with 1% osmium (OsO_4) and 1% potassium ferricyanide [$FeK_3(CN)_6$] in 0.1 M sym-collidine-HCl buffer (pH 7.4) rinsed with 0.1 M maleate buffer (pH 7.4) in 5% EDTA in 0.1 M phosphate buffer (pH 7.4–7.8), with gentle shaking for 48–72 h at 4 °C to soften remaining bone. Tissues were embedded in araldite and then sectioned at 40 μm parallel to the cochlear modiolus. These thick sections were reembedded in Epon between Aclar sheets (EMS). Chosen sections were cut out under a dissecting microscope and then reembedded in Epon blocks for ultrathin sectioning (Leica Ultracut S) parallel to the modiolar axis. Several serial sections (65 nm thick) were collected onto Formvar-coated slot grids for image acquisition at a magnification of 30,000× on a Hitachi H7600 transmission electron microscope operating at 80 kV. Digital images (2,120 × 2,120 pixels) were collected at a 16-bit depth and analyzed as 8-bit files. Images were imported into Reconstruct software (73) for assembly, calibration, and alignment. The outlines of the hair cell and efferent and afferent neuronal contacts, as well as the postsynaptic cistern, presynaptic ribbons, and associated vesicles, were traced. The dimensions of objects and interobject distances were computed in three dimensions within the Reconstruct software. Three IHCs were reconstructed from two different rats.

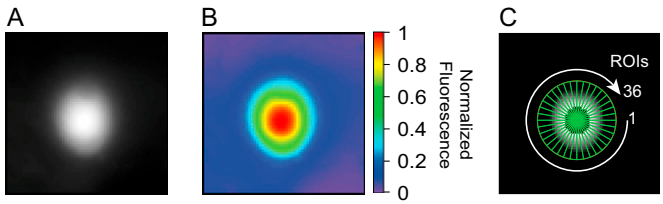

Fig. S1. ROI design scheme. (*A*) Average of all of the images acquired for a single IHC. (*B*) False color image of the picture depicted in *A* normalized to its maximum pixel value. (*C*) Radius comprising 0.4–0.9 relative cell fluorescence intensity was divided into 36 radial ROIs across the IHC cytoplasm.

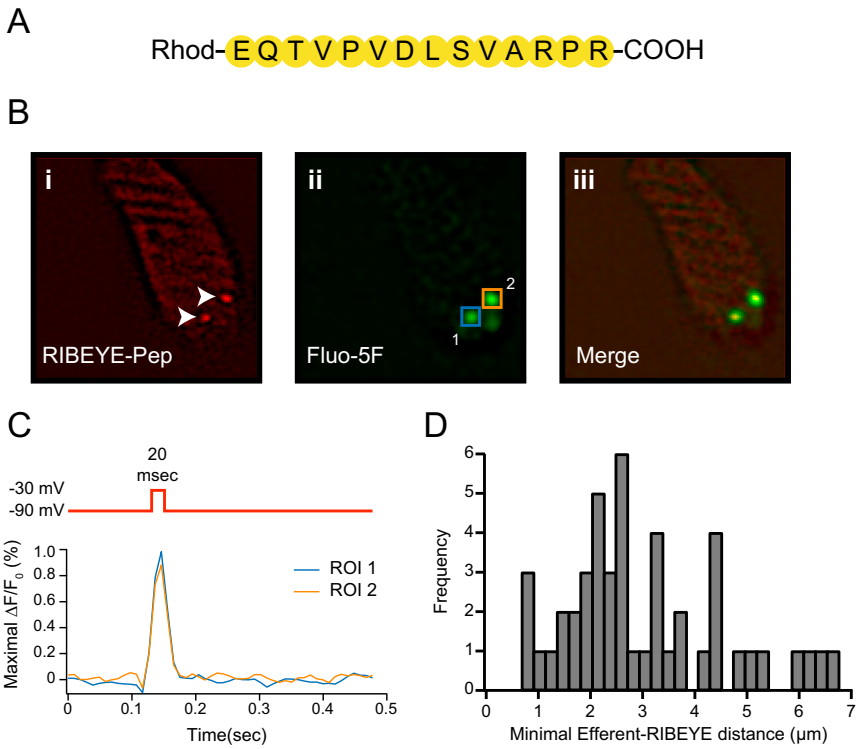

Fig. S2. RIBEYE peptide signal colocalizes with afferent Ca^{2+} entry sites. (*A*) Amino acid sequence of the fluorescent peptide used in this study. Rhodamine (Rhod) was attached to the N-terminal amino acid. (*B*) Swept-field confocal images of an IHC loaded with the rhodamine-labeled peptide and Fluo-5F. (*i*) RIBEYE peptide (Pep) signal obtained using a 561-nm laser. Arrowheads indicate RIBEYE puncta. (*ii*) Peak Ca^{2+} signal obtained during 20 ms of depolarization to −30 mV. (*iii*) Merge of images *i* and *ii*. (*C*) Fluorescence signal [$\Delta F/F_0$ (%)] measured in ROIs depicted in the image in *ii* during a 20-ms depolarization to −30 mV. (*D*) Frequency histogram obtained with all of the distances from each efferent hotspot to the closest RIBEYE puncta.

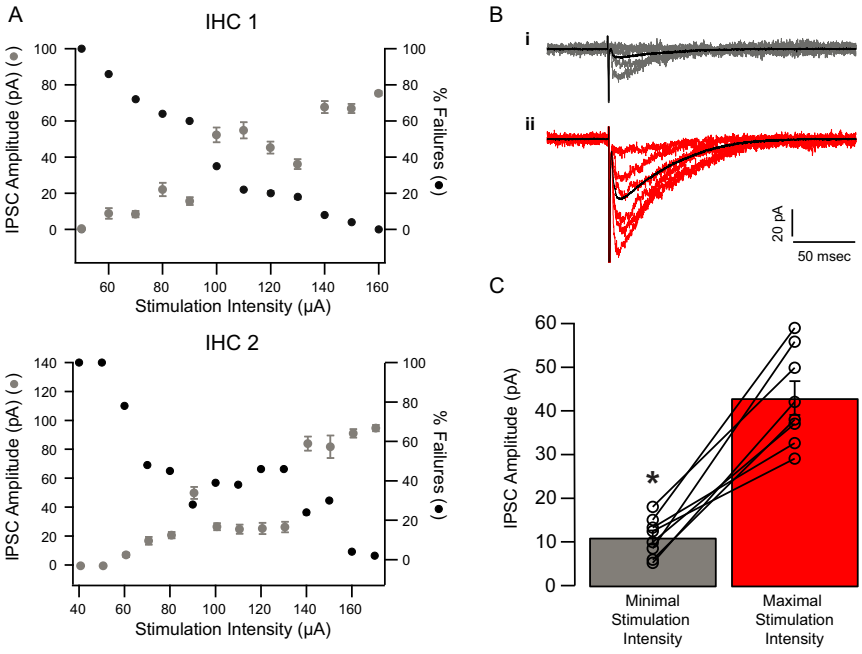

Fig. S3. Estimated number of converging efferent fibers using minimal-maximal stimulation protocols. Related to Fig. 2. (*A*) Data from two different IHCs showing average IPSC amplitude (left axis) and the percentage of synaptic failures (right axis) as a function of electrical stimulation intensity (in 10-μA steps). The progressive increase in the average eIPSC and the reduction in the number of synaptic failures are likely attributable to the recruitment of efferent fibers as the stimulation intensity was increased. (*B*) Representative whole-cell current traces during minimal (*i*) and maximal (*ii*) electrical stimulation protocols. The black line represents the average of all of the trials in each condition. (*C*) Average IPSC amplitude measured after minimal and maximal stimulation intensity. Wilcoxon matched-pairs signed rank test, $*P = 0.0078$.

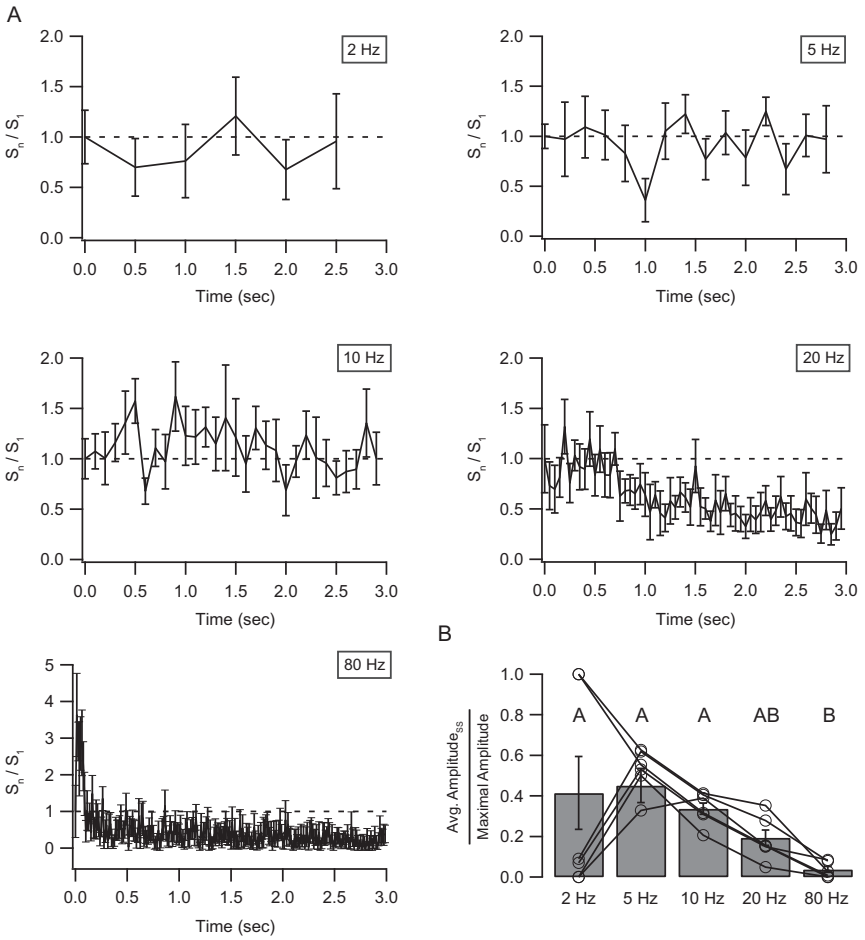

Fig. S4. High-frequency efferent stimulation produces synaptic depression. Whole-cell voltage-clamp recordings were made in P9–P11 mouse IHCs during trains of efferent electrical stimulation at different frequencies. Related to Fig. 4. (*A*) Amplitude of the response to each pulse during the train (S_n) was measured and normalized to the amplitude of the first pulse (S_1). The normalized mean values at the different stimulation frequencies are plotted versus the pulse number. Note that at high frequencies, there is a decrease toward the end of the train. (*B*) Average (Avg.) amplitude of IPSCs evoked during the last 0.5 s (steady state) of the stimulation protocol and normalized to the maximal response measured during the train. Each set of data points connected by lines represents a different cell. At 2 Hz, only the last pulse of the train was taken into consideration to average the steady-state amplitude. Different letters represent statistical differences. Friedman's test, $P < 0.01$.

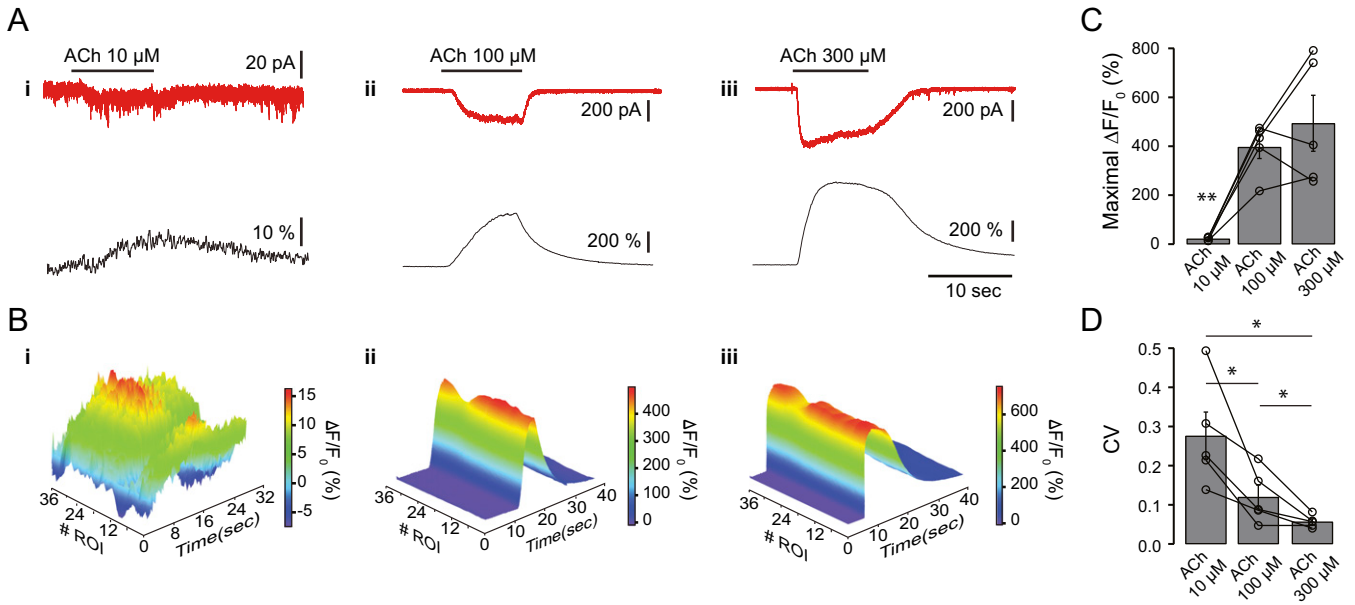

Fig. S5. Ca^{2+} influx produced by local application of ACh. IHCs were loaded with Fluo-4 (400 µM) and EGTA (500 µM) and illuminated with a blue LED in a wide-field microscope to measure the Ca^{2+} influx produced by local applications of the nAChR agonist ACh. Related to Fig. 4. (*A*) Representative current through α9α10 receptors (red) and fluorescence changes (black) produced by local applications of 10 (*i*), 100 (*ii*), and 300 (*iii*) µM ACh in the same IHC. (*B*) Three-dimensional representation of the fluorescence signal [$\Delta F/F_0$ (%)] as a function of ROI number (ROI design is discussed in *Methods*) and time during local applications of 10 (*i*), 100 (*ii*), and 300 (*iii*) µM ACh. (*C*) Maximal $\Delta F/F_0$ (%) during ACh applications: 21 ± 3 $\Delta F/F_0$ (%), 397 ± 47 $\Delta F/F_0$ (%), and 494 ± 114 $\Delta F/F_0$ (%) for 10 µM, 100 µM, and 300 µM ACh, respectively ($n = 5$ cells). Friedman test, $^{**}P < 0.01$. (*D*) Average CV of fluorescence changes across ROIs at the time point when the Ca^{2+} transient peaked: 0.28 ± 0.06, 0.12 ± 0.03, and 0.06 ± 0.01 for 10 µM, 100 µM, and 300 µM ACh, respectively ($n = 5$ cells). Friedman test, $^{*}P < 0.05$.

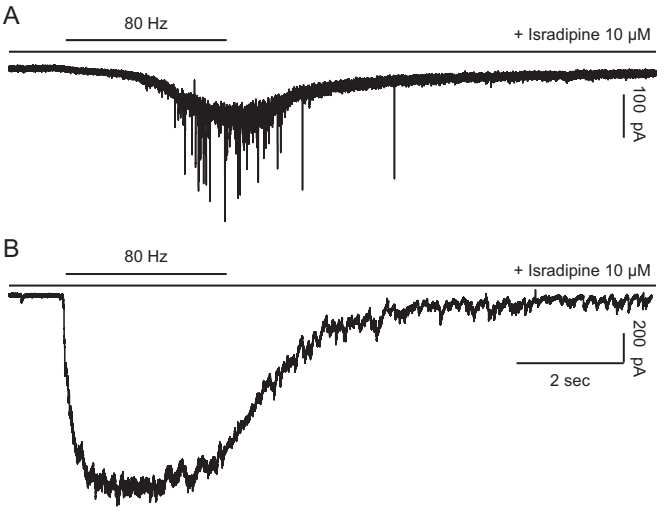

Fig. S6. Only one afferent bouton recording showed an increase in EPSC activation upon efferent stimulation. Voltage-clamp recordings from an afferent bouton during efferent stimulation. Related to Fig. 6. (*A*) Only recording that exhibited an increased EPSC rate when the MOC fibers were stimulated at 80 Hz for 3 s. (*B*) Trace depicts the synaptic response obtained in the IHC that lay presynaptic to the bouton shown in *A* during the same stimulation protocol. The accumulated charge was the largest found in these experiments.

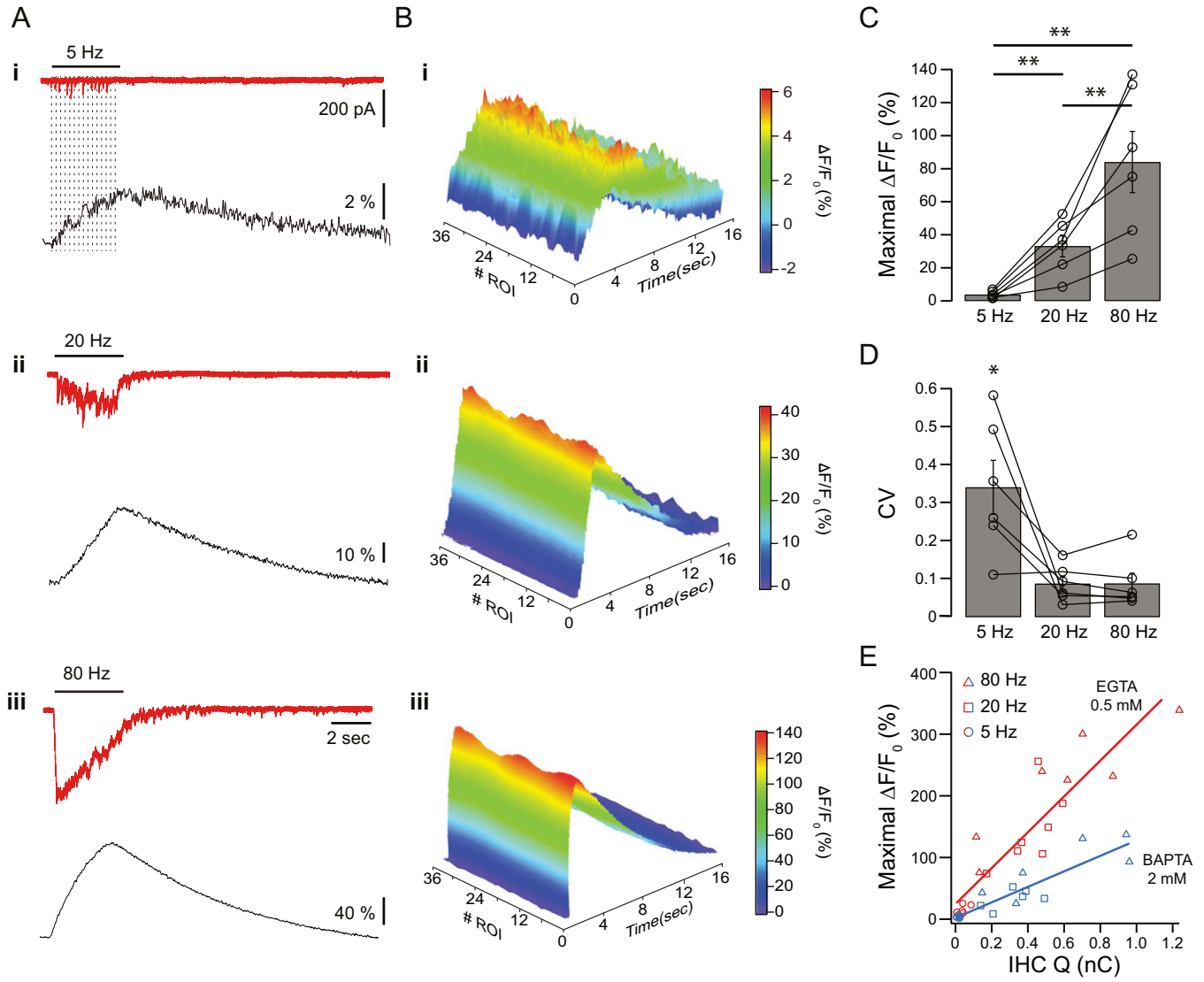

Fig. S7. Ca^{2+} influx produced by trains of efferent stimuli in IHCs loaded with BAPTA. IHCs were loaded with Fluo-4 (400 μM) and BAPTA (2 mM), and Ca^{2+} influx produced by trains of efferent stimuli was measured using blue LED wide-field illumination. (*A*) Representative synaptic responses (red traces) and changes in fluorescence [black traces, expressed as $\Delta F/F_0$ (%)] produced in the same IHC during a 3-s electrical stimulation of efferent fibers at 5 (*i*), 20 (*ii*), and 80 (*iii*) Hz. (*B*) Three-dimensional representation of the fluorescence signal [$\Delta F/F_0$ (%)] as a function of ROI number (ROI design is discussed in *Methods*) and time during electrical stimulation of efferent fibers at 5 (*i*), 20 (*ii*), and 80 (*iii*) Hz. (*C*) Maximal $\Delta F/F_0$ (%) reached during efferent stimulation trains: 5 Hz = 3.8 ± 0.8 $\Delta F/F_0$ (%), 20 Hz = 33.2 ± 6.4 $\Delta F/F_0$ (%), and 80 Hz = 84.1 ± 18.5 $\Delta F/F_0$ (%). Friedman's test, $^{**}P < 0.01$ ($n = 6$). (*D*) Average CV of fluorescence changes across ROIs at the time point when the Ca^{2+} transient peaked: 5 Hz = 0.34 ± 0.07, 20 Hz = 0.09 ± 0.02, and 80 Hz = 0.09 ± 0.03. Friedman test, $^{*}P < 0.05$ ($n = 6$). (*E*) Correlation between maximal fluorescence change and the charge (Q) accumulated at the end of the stimulation protocol for IHCs loaded with EGTA 0.5 mM (red) or BAPTA 2 mM (blue). Spearman correlation, $P < 0.0001$. The best model fit supports different curves for each dataset. *F* test, $P < 0.0001$.

Table S1. Electrophysiological and fluorescence signal parameters obtained after single electrical stimulation of efferent fibers

Technique	Parameter	Value
Electrophysiology	No. of sweeps per cell	54.9 ± 6.3
	Successful events, %	71.8 ± 4.8
	IPSC amplitude, pA	80.1 ± 5.4
	IPSC charge, pC	3.0 ± 0.4
	τ_{decay}, ms	53 ± 6
	CV (excluding failures)	0.50 ± 0.03
Imaging	Hotspots per cell	2.6 ± 0.2
	Ca^{2+} transient amplitude, $\Delta F/F_0$ (%)	5.6 ± 0.6
	τ_{decay}, (ms)	135 ± 10
	CV (excluding failures)	0.43 ± 0.05
	Amplitude synaptic failures, $\Delta F/F_0$ (%)	0.5 ± 0.1
	Multiple hotspot probability*	37.4 ± 8.3
	Synaptic events with Ca^{2+} transients, %	44.0 ± 4.1

This table is related to Fig. 1.

*Multiple hotspot probability represents the chance of finding more than one hotspot provided that a fluorescence signal increase was detected.